Sources of secondary microseisms in the Indian Ocean

Céline Davy, Eléonore Stutzmann, Guilhem Barruol, Fabrice R. R. Fontaine, Martin Schimmel

Sources of secondary microseisms in the Indian Ocean

C. Davy,[1] E. Stutzmann,[2] G. Barruol,[1] F.R. Fontaine[1] and M. Schimmel[3]

[1]*Laboratoire GéoSciences Réunion, Université de La Réunion, Institut de Physique du Globe de Paris, Sorbonne Paris Cité, UMR CNRS 7154, Université Paris Diderot, 15 avenue René Cassin, CS 92003, F-97744 Saint Denis cedex 9, France. E-mail:* celine.davy@univ-reunion.fr
[2]*Institut de Physique du Globe de Paris, Sorbonne Paris Cité, UMR 7154 CNRS, Paris, France*
[3]*Institute of Earth Sciences Jaume Almera, CSIC, Lluis Sole i Sabaris s/n, E-08028 Barcelona, Spain*

SUMMARY

Ocean waves activity is a major source of microvibrations that travel through the solid Earth, known as microseismic noise and recorded worldwide by broadband seismometers. Analysis of microseismic noise in continuous seismic records can be used to investigate noise sources in the oceans such as storms, and their variations in space and time, making possible the regional and global-scale monitoring of the wave climate. In order to complete the knowledge of the Atlantic and Pacific oceans microseismic noise sources, we analyse 1 yr of continuous data recorded by permanent seismic stations located in the Indian Ocean basin. We primarily focus on secondary microseisms (SM) that are dominated by Rayleigh waves between 6 and 11 s of period. Continuous polarization analyses in this frequency band at 15 individual seismic stations allow us to quantify the number of polarized signal corresponding to Rayleigh waves, and to retrieve their backazimuths (*BAZ*) in the time–frequency domain. We observe clear seasonal variations in the number of polarized signals and in their frequencies, but not in their *BAZ* that consistently point towards the Southern part of the basin throughout the year. This property is very peculiar to the Indian Ocean that is closed on its Northern side, and therefore not affected by large ocean storms during Northern Hemisphere winters. We show that the noise amplitude seasonal variations and the backazimuth directions are consistent with the source areas computed from ocean wave models.

Key words: Surface waves and free oscillations; Indian Ocean.

INTRODUCTION

Microseismic noise is generated by ocean gravity waves (Longuet-Higgins 1950; Hasselmann 1963) and is recorded worldwide by broadband seismic stations in the frequency range 0.05–0.3 Hz (periods between ∼3 and 20 s). It is associated to ground vibration of a few microns in amplitude, and has been used in early investigations of seismic noise sources because it is correlated with weather disturbances (e.g. Banerji 1930). Microseismic noise is dominated by Rayleigh waves (e.g. Ramirez 1940), but body waves were also observed and modelled (e.g. Barruol *et al.* 2006; Gerstoft *et al.* 2008; Koper *et al.* 2010; Gualtieri *et al.* 2014). Microseisms are generally split into primary (PM) and secondary microseisms (SM) that result from different physical processes. PM have the same periods as the ocean swells (typically between 10 and 20 s) and are accepted to be generated through direct interaction of swell with the sloping seafloor in coastal areas (Hasselmann 1963). SM, on which we focus this work, dominate seismic noise worldwide. They have half the period of the ocean waves (typically between 3 and 10 s) and are induced by a second-order pressure fluctuation generated by interference of swells of similar periods travelling in opposite directions (Longuet-Higgins 1950).

It has long been known that SM are dominated by Rayleigh waves in the frequency range 0.1–0.17 Hz (6–10 s of period; Lee 1935; Lacoss *et al.* 1969; Tanimoto & Alvizuri 2006) that can be observed on seismic stations far from their generation areas (e.g. Haubrich *et al.* 1963; Tanimoto *et al.* 2006), but recent studies have shown that Love wave (Nishida *et al.* 2008; Tanimoto *et al.* 2015) and compressional waves (Davy *et al.* 2014) can be detected in the SM frequency band. SM generally show elliptical polarization in the vertical plane, so the direction to the incoming waves can be inferred from the polarization observed on individual seismic stations, under the assumption that they are surface waves with retrograde polarization. SM noise sources have been located in near-coastal shallow waters (e.g. Bromirski *et al.* 2013), related to coastal swell reflections interacting with the incident swell (e.g. Bromirski & Duennebier 2002) and also in deep waters (e.g. Obrebski *et al.* 2012), related to interactions between swells of opposite directions and similar periods. Most of the literature on the SM noise sources focuses on the Pacific and Atlantic oceans (e.g. Haubrich & McCamy 1969; Friedrich *et al.* 1998; Chevrot *et al.* 2007; Gerstoft & Tanimoto 2007; Brooks *et al.* 2009; Koper *et al.* 2010; Behr *et al.* 2013) or on the global scale (Aster *et al.* 2008; Gerstoft *et al.* 2008; Stutzmann *et al.* 2012) and very few on the Indian

(e.g. Koper & De Foy 2008; Sheen 2014) and the Southern oceans (e.g. Reading *et al.* 2014). The motivation of this work is therefore to improve our knowledge of the noise sources in the Indian Ocean.

SM source regions have been remotely detected and located in the ocean basins by techniques such as beamforming (e.g. Essen *et al.* 2003; Landès *et al.* 2010) or polarization analyses (e.g. Schimmel *et al.* 2011), and also modelled (e.g. Ardhuin *et al.* 2011; Stutzmann *et al.* 2012). From numerical modelling, Ardhuin *et al.* (2011) showed that seismic sources generated on the seafloor by standing waves developing at the ocean surface may occur under three situations of ocean–wave interactions: in a single storm with a broad ocean wave directional spectra (class I), by the interaction between an incoming swell with its own coastal reflection (class II), and finally, by two distinct swells of similar periods and propagating in opposite directions (class III).

In this study, we used 1 yr (2011) of continuous data recorded at 15 permanent broad-band seismic stations located in the Indian Ocean basin. The choice of this particular year was motivated by the data continuity provided at most stations and the time length of 1 yr was chosen to spot seasonal variations. On these continuous data, we performed a polarization analysis (Schimmel & Gallart 2003, 2004, 2005; Schimmel *et al.* 2011) to detect polarized signals in the time-frequency domain and to determine their backazimuths (*BAZ*). We then used this information to characterize the source areas of SM noise in the Indian Ocean and to follow their variations with time and frequency. Finally, we compared the results obtained by the polarization analysis with the locations of the SM noise sources predicted by a numerical wave model.

DATA AND METHOD

We processed 1 yr (2011) of continuous waveform data from 15 seismic stations of global (GEOSCOPE, GSN) and regional seismic networks (Geoscience Australia, Pacific21) located in the Indian Ocean (Fig. 1). These stations were selected for their complete geographical distribution and their good data availability during the year 2011. Data from the three components (north–south, east–west and vertical) were converted to ground velocity by removing the instrument response and decimated at 1 sample per second to extract frequency-dependent noise polarization from the continuous three-component records in the frequency range 0.05–0.33 Hz (between 3 and 20 s of period). All individual records were transformed into the time-frequency domain using the *S* transform (Stockwell 1996; Ventosa *et al.* 2008) in which the window size has been scaled to the period of interest.

We performed a polarization analysis (Schimmel & Gallart 2003, 2004, 2005; Schimmel *et al.* 2011) that allows detecting polarized signals as a function of time and frequency, which are characterized by the measurement of the instantaneous degree of polarization (DOP). The DOP is a quality measurement linked to the stability of an arbitrary polarization state with time. It is based on the fact that the polarization of a high-quality signal should remain stable with time. The DOP has been adjusted to detect elliptical particle motion in a vertical plane and is built from polarization attributes, such as the semi-major and semi-minor axes of the ellipse that best fit the ground motion. It ranges between 0 and 1, with 1 indicating a perfect polarized signal of elliptical particle motion in a vertical plane and 0 a random ground motion. The polarization attributes are determined through an eigen analysis of spectral matrices which were constructed from the time–frequency representation of the
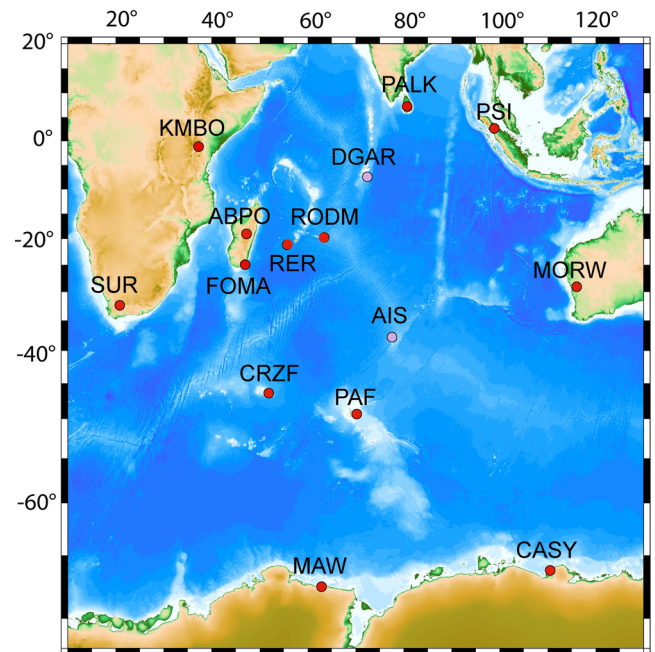

Figure 1. Map of the 15 permanent Indian Ocean seismic stations used in this work. These stations are part of the GEOSCOPE, IRIS, Geoscience Australia and Pacific21 networks. The station locations are indicated by coloured circles to indicate if the dominant noise is in the PM (light purple) or SM (red) frequency bands (see Fig. 2).

three component seismograms. For more details about the DOP construction see Schimmel *et al.* (2011).

Detections were based on DOP larger than 0.75 to keep only the measurements corresponding to stable elliptical polarization but also on the polarization stability over a time period of a minimum four times the signal period. Combining this polarization with the fact that the orientation of the ground motion ellipse is assumed to be retrograde, as described for fundamental mode Rayleigh waves, allows us to determine the direction of the incoming waves, called the *BAZ*.

This polarization analysis resulted in a matrix containing time, frequency, DOP and *BAZ* quadruples for all the signals detected during the year at each seismic station. These data are then used to analyse the *BAZ* of the seismic sources in the Indian Ocean and their variations with time and frequency.

RESULTS OF POLARIZATION ANALYSIS

We first quantified the amount of elliptically polarized signals detected throughout the year at each station as a function of frequency. We obtained the polarization spectra shown in Fig. 2, in which the black bold lines represent the amount of polarized signals counted in frequency bins of 0.01 Hz. The maximum number of detected signals by bins was normalized to 1 at each station to show the relative distribution of the polarized signals as a function of frequency.

All the polarization spectra clearly show a bimodal distribution with a frontier between the two peaks around 0.09 Hz (11 s of period). The histogram superimposed on every plot in Fig. 2 indicates for each station the normalized total amount of detections throughout the year in each frequency band. One observes generally much less polarized signals for the PM (in light purple, between 0.04
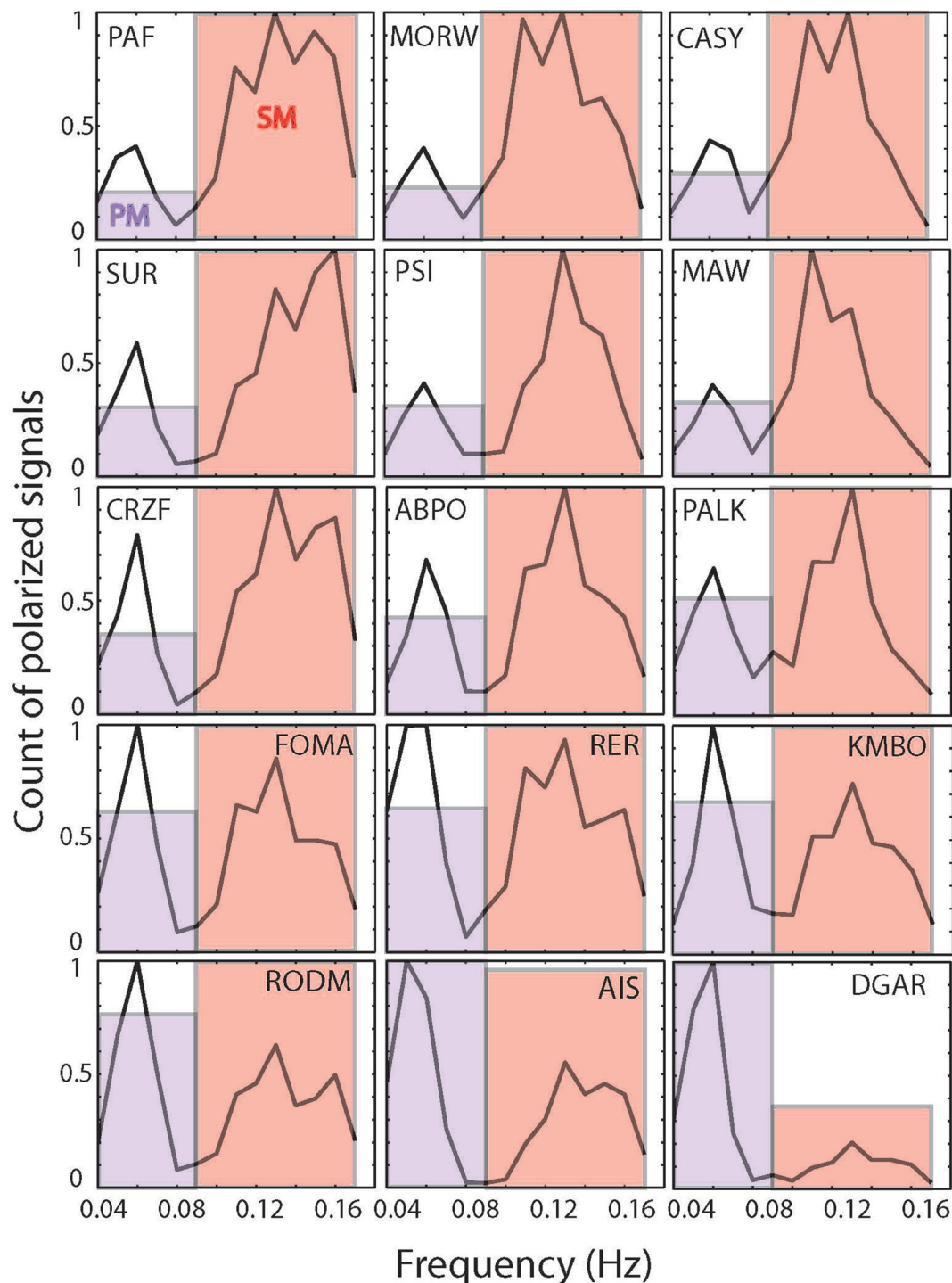
Figure 2. Polarization spectra showing the distribution of the polarized signals detected throughout the year 2011 as a function of frequency for the 15 Indian Ocean stations. PM marks the primary microseism frequency band between 0.04 and 0.09 Hz (around 11–25 s) and SM marks the secondary microseism frequency band between 0.09 and 0.17 Hz (around 6–11 s). A histogram is superimposed on each plot and shows the normalized relative distribution between the polarized signals counted throughout the year in the PM (in light purple) and the SM (in red) frequency bands. The stations are sorted on the relative importance of the SM over the PM magnitude.

and 0.09 Hz, 11–25 s of period) than for the SM (in red, between 0.09 and 0.17 Hz, 6–11 s of period). We thus observe more polarized signals detected in the SM frequency band at most stations, whatever their land, coastal or island situation. The PM detections dominate only at stations DGAR and slightly at AIS. However, it must be noted that these two seismic stations seem to be of low

quality with particularly noisy data (as discussed later) that could make the detection of both the PM and SM less robust.

The variations of the number of detections in time reveal a clear seasonality for the SM detections, whereas PM detection levels are rather constant throughout the year, as shown in Fig. 3. More SM polarized signals are detected in austral winter (from May to
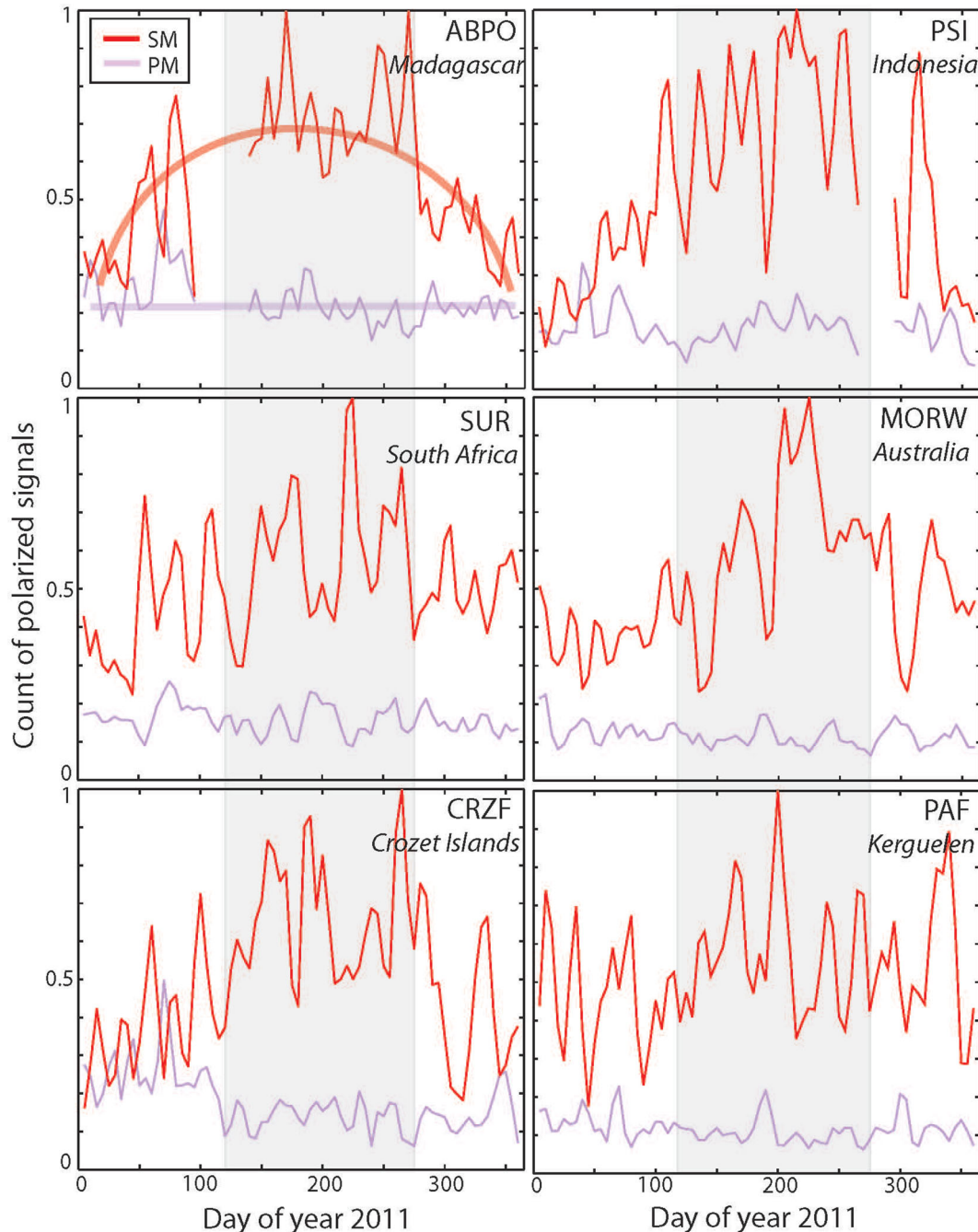
Figure 3. Seasonal variations of the number of detected signals polarized in a vertical plane throughout the year 2011 at the stations ABPO (Ambohimpanompo, Madagascar), PSI (Sumatera, Indonesia), SUR (Sutherland, South Africa), MORW (Morawa, Western Australia), CRZF (Port Alfred-Ile de la Possession-Crozet Islands, France) and PAF (Port aux Français, Kerguelen Islands). Plotted are the normalized moving averages obtained from 10-d data windows with 50 per cent overlap. Frequency bands for the PM (in light purple) and the SM (in red) are the same as in Fig. 2. Austral winter is shaded in grey, from May to September.

September) at all these stations, even at the ones that are located in the Northern Hemisphere such as the station PSI. This feature can be explained by the fact that the Indian Ocean is closed on its Northern side and is therefore dominated by a Southern Hemisphere dynamics. All the stations in and around this ocean record many more polarized signals in austral winter than in austral summer (December to March). This is not the case for the seismic stations located in the Atlantic or the Pacific oceans. These basins indeed extend at high latitudes in both the Northern and Southern Hemispheres, where Northern and Southern winter storms may de-

velop. In these oceans, one observes a variability of the SM over the year correlated with the latitude of the stations and the season, with more SM signals during the local winter in both Northern and Southern Hemispheres (e.g. Stutzmann *et al.* 2009; Schimmel *et al.* 2011).

To localize the SM source generation areas, we use the *BAZ* measured at each individual seismic station by the polarization analysis. The *BAZ* are extracted from the elliptically polarized signals with particle motion in a vertical plane. The 180° ambiguity in the *BAZ* is removed by assuming that fundamental mode surface waves are

Figure 4. Monthly variations of SM polarized signals detected at stations ABPO and PAF throughout the year 2011. Every polarization diagram corresponds to one month of measurements where each detection is characterized by its backazimuth (indicated by the angle with respect to north) and its frequency (indicated by the radius). Inner and outer circles correspond to 0.09 and 0.17 Hz (around 6–11 s), which are the limits of the SM frequency band. The colour indicates the number of polarized signals detected by bin of 3° for the backazimuth and of 0.01 Hz for the frequency. Red colours correspond to the maximum number of SM polarized signals detected by bins, which is saturated at 500.

characterized by a retrograde polarization. The polarization analysis is performed in the time-frequency domain, and we can therefore measure the *BAZ* as a function of time and frequency.

Fig. 4 shows examples of the monthly variations of the SM *BAZ* as a function of frequency at station ABPO in Madagascar and PAF in Kerguelen Islands. These two stations exhibit different SM detection patterns, but they both show a dominant *BAZ*, stable throughout the year. Detections at station ABPO point to a source area localized towards the south–southeast of Madagascar whereas detections at station PAF point out towards the west–southwest of the Kerguelen Islands. The seasonal variability in the number of SM polarized signals is underlined by much more detected signals during the austral winter than during the austral summer. As a comparison, the total amount of SM signals detected in the frequency band 0.09–0.17 Hz at station PAF was 65 699 in July and only 36 925 in February.

We also observe a seasonal variability in the dominant frequency of the SM signals throughout the year, with higher frequency SM signals detected in austral summer and lower frequency SM signals detected in austral winter. This feature visible on the two examples presented in Fig. 4 is found at most seismic stations and summarized in Fig. 5, which represents the daily dominant measured frequency of the SM polarized signals at ten stations throughout the year 2011, smoothed over a week-long moving window. Despite the fact that each curve may display important variations of 10–30 d of period, Fig. 5 clearly shows a general trend characterized by a yearly variation, with lower dominant frequencies for signals detected during austral winter (indicated by the grey area) and higher dominant frequencies for signals detected during austral summer. Such a seasonality of the SM dominant frequency can be explained by the fact that the largest storms, characterized by long period swells, occur mainly in austral winter, and thus generate longer period SM (with half the period of the ocean waves).

This year-long analysis also reveals a dominant *BAZ* in the SM frequency band that remains stable throughout the year at most seismic stations within and around the Indian Ocean basin. This stability allows us to investigate the geographical meaning of the SM noise source locations. Fig. 6 shows the detection pattern of the polarized signals in the SM frequency band (0.09–0.17 Hz) for the entire year 2011 at each seismic station, using the same representation as in Fig. 4, except that the number of polarized signals has been normalized to 1 for each seismic station. The colour scale has been saturated so that bins above 0.5 are shown in dark red to increase the visibility of smaller amplitude features.

Most seismic stations show clear and dominant *BAZ* sources for the SM polarized signals throughout the year. The main directions of the dominant *BAZ*, corresponding to the maximum of polarized signals counted in the SM frequency band, are delimited in Fig. 6 by black lines centred on the location of the seismic station. This clearly shows that the dominant *BAZ* generally points towards the South of the Indian Ocean.

This systematic analysis also shows that the stations DGAR, RODM and AIS appear to be of low quality, probably owing to a noisier environment. For these three stations, the majority of the polarized signals cover a large domain pointing globally from the southwest to the southeast but without any stable and dominant *BAZ* throughout the year. The power spectral density (PSD) estimates at these stations (available at the Geoscope website http://geoscope.ipgp.fr and IRIS website http://ds.iris.edu/ds/products/pdf-psd/) show a noise level in the SM frequency band higher than the new high-noise model (NHNM; Peterson 1993), which may explain the weak performance of these broadband stations in detecting polarized signals.

If most stations show only one dominant range of *BAZ*, exceptions are observed at stations CRZF, CASY and PALK. For these three stations, we found a dominant *BAZ* that points towards the Southern
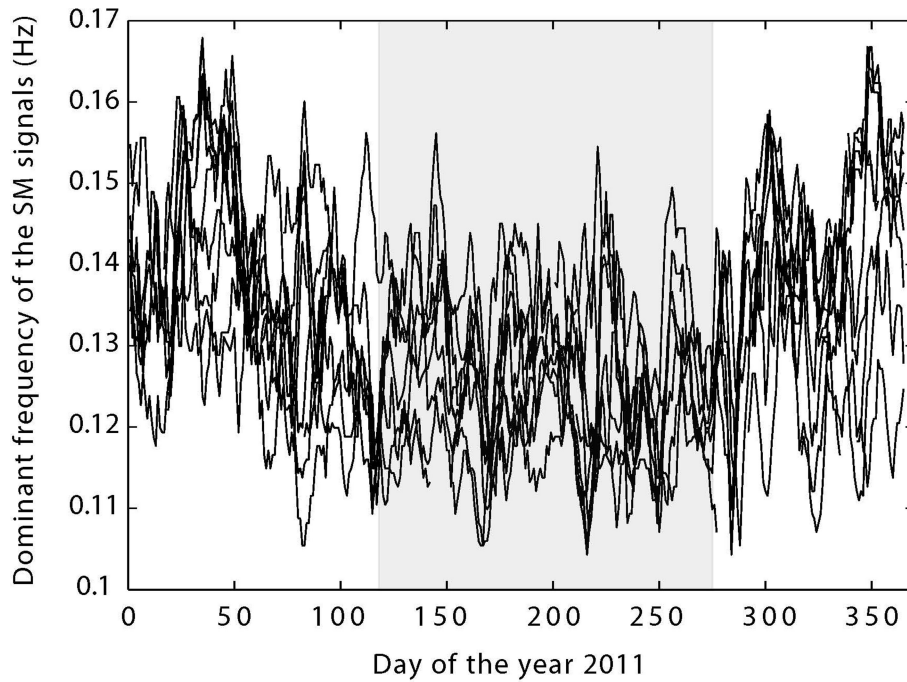
Figure 5. Seasonal variation of the dominant frequency of the SM, as a function of the day of year 2011 for 10 of the Indian Ocean seismic stations. We plot the dominant frequency of the SM polarized signals within each day with a smoothing window spanning one week. Austral winter is shaded in grey, from May to September.
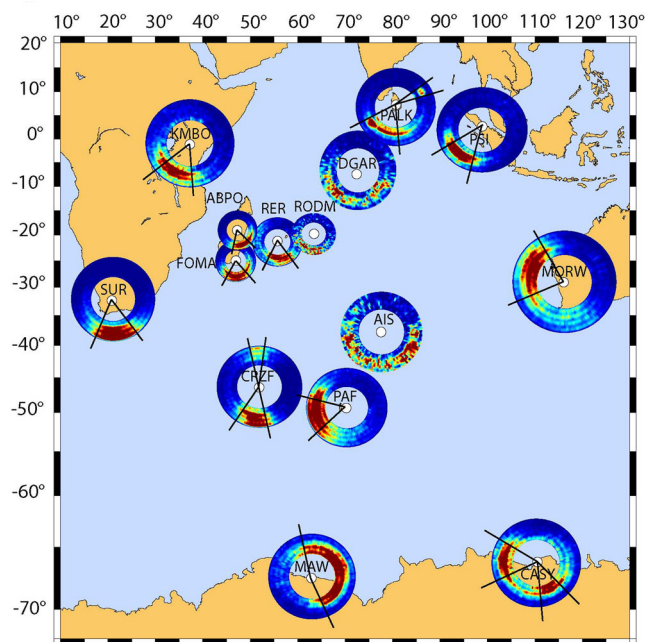

Figure 6. Detection of the SM polarized signals throughout the year 2011. Diagrams are similar to those of Fig. 4 except that they cover the whole year. Black lines delimit the dominant directions of the noise source backazimuths measured at each seismic station.

Indian Ocean, but also a secondary *BAZ* which points to a clearly different direction. At station CRZF, a second source of SM noise is likely present north of Crozet Islands. At CASY, SM coming from the southeast likely result from a source area located in the Southern Pacific Ocean and at station PALK, secondary noise sources point towards the northeast, likely towards the Bay of Bengal, as observed previously by Koper *et al.* (2008).

Another distinct feature is observed at station MORW, in Western Australia, where the dominant *BAZ* detected does not point towards the Southern Indian Ocean, but instead towards the northwest. A likely hypothesis to explain detections at this station is that the SM sources could be dominated by swell coastal reflections rather than distant ocean waves interaction. This is favoured by the fact that noise source modelling shows that strong SM sources are generated by wave reflections at the Western coast in Australia (Stutzmann *et al.* 2012). This point is discussed below and illustrated in Fig. 7.

DISCUSSION

PM versus SM amplitudes

The PM and SM are both characterized by large amounts of elliptically polarized signals but at most stations, we detected more signals in the SM frequency band than in the PM one throughout the year (Figs 2 and 3). This can be explained by the fact that the SM are observed globally as the strongest microseisms (e.g. Aster *et al.* 2008), but also because they are detected in a larger frequency band, and because the mechanism at the origin of the SM can occur in both shallow waters and deep ocean. In contrast, the smaller number of PM detections can be explained by its narrower frequency band, but also by the fact that they are generated in shallow waters through pressure variations on the sloping seafloor and are quickly attenuated with distance (e.g. Barruol *et al.* 2006).

SM of classes I and III (Ardhuin *et al.* 2011), that are generated by more distant source areas located in the deep ocean can explain both the predominance of the SM over the PM, and the seasonal variations in SM with more energy during austral winter when larger storms occur in the southern ocean. If the SM of class II (generated near the shore by coastal reflection of an incoming swell) were responsible for the SM increase detected during austral winter, we should observe a simultaneous PM increase at the same time, since
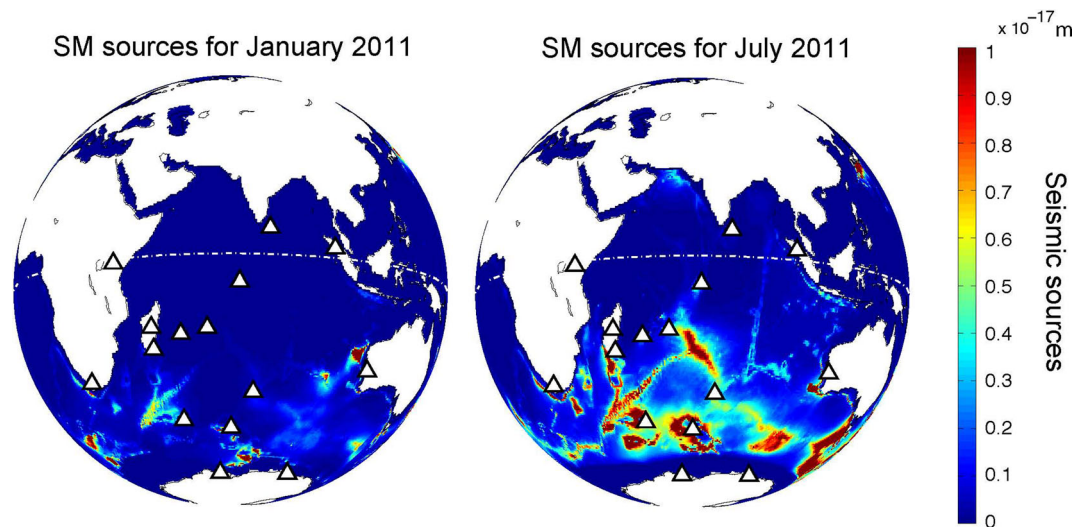
Figure 7. Maps of the SM sources in January 2011 (left-hand side) and July 2011 (right-hand side), modelled with a 10 per cent coefficient of ocean wave coastal reflection. The Equator is represented by the white dotted line. See text for interpretation.

the PM are also generated by the local swell activity near the shore. The missing seasonality in the PM observations suggests that PM and SM are decoupled from each other as one may expect for distant SM sources and near-coastal PM sources. The absence of seasonal variability in the number of detected signals in the PM frequency band (Fig. 3) suggests that the stations record SM signals predominantly from distant source areas of classes I and III located in the deep ocean. Since the SM have twice the frequency of the ocean waves generating them and are proportional to the product of their amplitudes (Longuet-Higgins 1950), one can expect an increase in the number of SM polarized signals and also a lower dominant frequency of the SM during austral winter, when large swell events with longer periods occur in the Indian Ocean (as shown in Figs 4 and 5).

Location of SM noise sources

As the SM *BAZs* are stable in time, we used the *BAZs* detected throughout the year 2011 at each individual station to investigate potential SM noise source areas (Fig. 6). Most of the measured *BAZs* point to the South of the oceanic basin for the SM, which is consistent with the fact that fewer noise sources can be generated in the Northern Indian Ocean which is closed by continent with respect to the open Southern Indian Ocean. This is furthermore confirmed by the much larger number of polarized signals detected in austral winter, even at the Indian Ocean stations located in Northern Hemisphere, such as station PSI.

Although the main sources are located in the Southern Indian Ocean, we show that a few stations are also sensitive to noise sources located in other oceans. For example, the Antarctica stations MAW and CASY point towards source areas in the Southern Pacific Ocean.

The station MORW seems to be sensitive to SM sources induced by coastal reflections rather than distant sources. This station detected a large number of polarized signals with *BAZ* pointing towards the northwest and not towards the southern area of the Indian Ocean. Owing to the closed geometry of the Indian Ocean in its northern part, seismic sources of class I or III related to deep ocean sources (Ardhuin *et al.* 2011) are less expected in the northwest of Australia. This may indicate that the sources detected by the station MORW are likely induced by coastal reflection processes.

SM noise sources observations versus modelling

In order to validate the locations of the SM source areas issued from our polarization measurements, we compared these locations with the noise sources predicted by the numerical wave model IOWAGA (Ardhuin *et al.* 2010, 2011). SM sources are generated at places where opposite travelling ocean wave trains with the same frequency meet. The interaction of these swells generates standing or partially standing waves that induce pressure fluctuations on the ocean bottom through the water column, at twice the ocean wave frequency, which efficiently couple into seismic energy on the seafloor. These sources are modelled by integrating local ocean wave spectra over all azimuths combined with a site effect, which corresponds to the resonance effect in the water column (Longuet-Higgins 1950; Kedar *et al.* 2007; Stutzmann *et al.* 2012; Gualtieri *et al.* 2013). For details of the numerical modelling and theory see Ardhuin *et al.* (2011) and Stutzmann *et al.* (2012).

Fig. 7 shows the maps of the noise sources modelled in the SM frequency band for the months of January and July 2011, using the same colour scale. The source maps are computed for the same frequency range as those used for the polarization analysis, that is, between 0.09 and 0.17 Hz for the SM. According to the models, the strongest SM sources are mainly localized both in deep-ocean and in the Southern part of the basin, where crossing wave fields are more common, and they have more energy in July, when the largest storms occur. Fig. 7 also reveals the amplification of SM sources due to resonance effect, which depends on water depths (Longuet-Higgins 1950). This explains why SM sources are clearly distributed along topographic features such as the Indian mid-oceanic ridges, the Kerguelen and the Madagascar plateaus. The optimum ocean depth for the excitation of microseisms varies for different frequencies (e.g. Longuet-Higgins 1950; Kedar *et al.* 2007; Stutzmann *et al.* 2012; Gualtieri *et al.* 2013; Tanimoto 2013) and is for example of 2.7 km for 0.15 Hz. Noise in the SM frequency band is particularly well excited at ocean depth of about 2–3 km, which is in good agreement with the distribution of the modelled SM sources shown in Fig. 7.

These modelled noise sources clearly favour the dominant SM activity during austral winter and also the distant origin of the sources for the generation of the SM in the Indian Ocean. The SM source areas that we observe are characterized by large patches located in
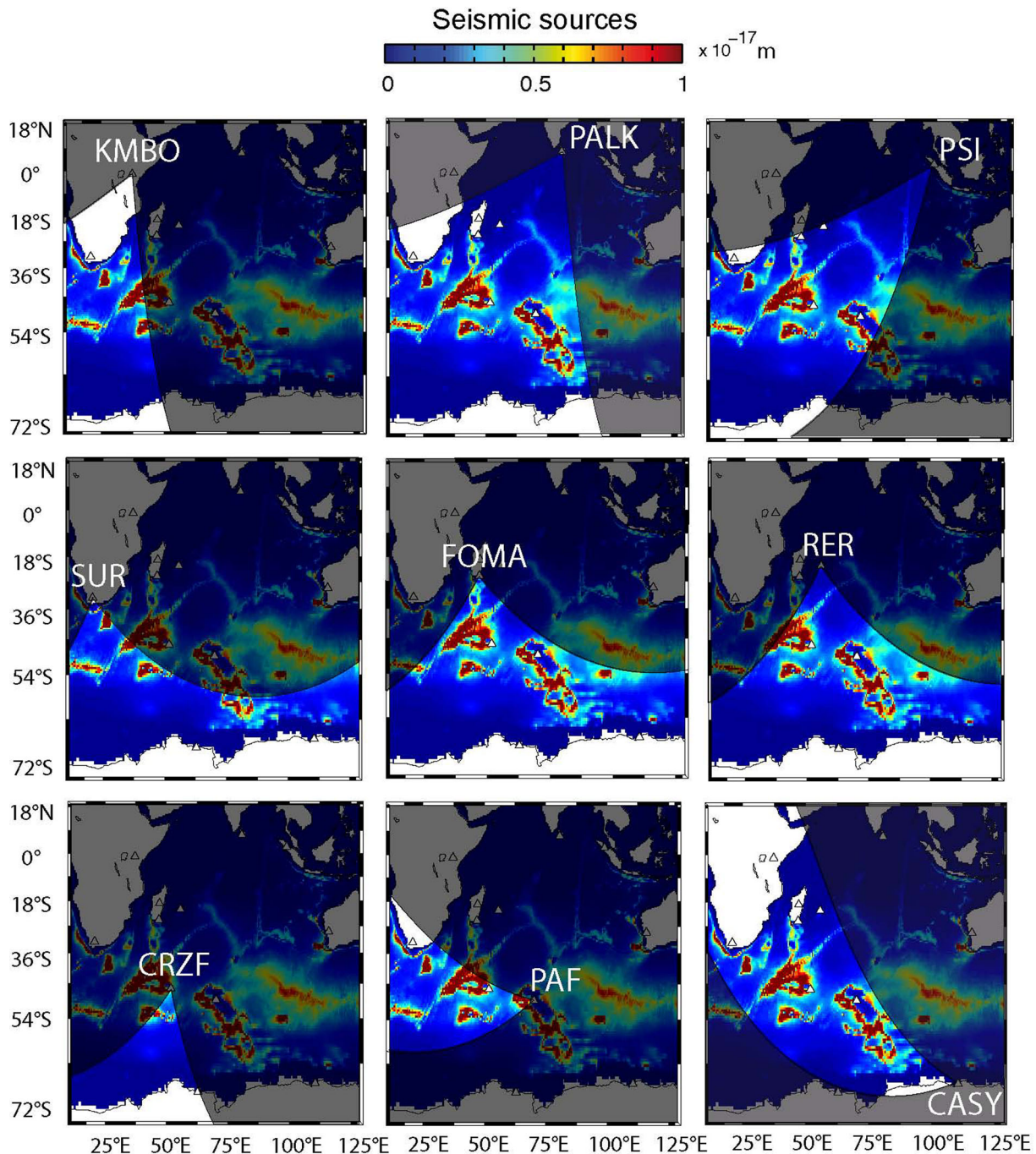
Figure 8. Maps of the dominant measured backazimuth at most of the stations, superimposed on the SM sources modelled for the year 2011 with a 10 per cent coefficient of ocean wave coastal reflection. See text for interpretation.

the Southern Indian Ocean and with clearly higher amplitude during austral winter, that is, when the larger storms occur.

The distribution of the SM sources computed from the global ocean wave model for the whole year 2011 is presented on the maps in Fig. 8. We highlight the projection of the measured *BAZ* from each seismic station averaged for the year, as delimited by black lines in Fig. 6. We only represent on this figure the seismic stations for which we measure a dominant and stable *BAZ* over the year, which points towards SM source areas located in the Indian Ocean. For that reason, we do not represent the low quality stations DGAR, RODM and AIS. The station ABPO is also not presented on this figure, because it shows very similar results to stations FOMA

and RER. We also do not represent the station MORW in Australia where the dominant *BAZ* points towards the northwest suggesting local SM sources induced by coastal reflection that coincide well with an elongated zone of source area modelled along the Western coast of Australia.

Fig. 8 demonstrates that the polarization directions measured at most stations correlate well with the SM sources modelled in the South of the Indian Ocean. At most recording sites, we show a good agreement between the projections of the measured *BAZ* highlighting the South of the Indian Ocean and the modelled noise sources. Fig. 8 also reveals that some modelled source areas are not detected by our measurements. We suggest that there may be simultaneous

sources occurring in different areas and therefore spread over wide azimuths (Gerstoft & Tanimoto 2007). Simultaneous wave arrivals from different sources at a recording station may modify and complicate the polarization and we likely measure the strongest sources in our signal, explaining why some sources may be missed. Finally, one must keep in mind that the *BAZ* measured on individual seismic stations give information on the source direction but not on the source distance. The approach developed here therefore provides statistical information on the noise sources at large time and space scales. It allows characterizing and monitoring the climate-induced microseisms, but does not allow locating individual seismic sources. Deployment of ocean bottom seismometers using a station spacing smaller than the one used in the present work may provide a way to locate these local noise sources and to make *in situ* microseismic noise observations beneath oceanic storms in both deep and shallow waters (e.g. Webb & Crawford 2010). This was done for instance from data recorded by the RHUM-RUM experiment (Barruol & Sigloch 2013) that allowed observing SM sources on the ocean floor beneath a tropical cyclone (e.g. Davy *et al.* 2014). Another alternate way locating noise sources can be provided by methods such as spectral analyses that can be performed on individual stations. Investigation of PM and SM during a particular major storm may provide a way to determine the distance to the source, thanks to the dispersion of the ocean waves (Bromirski *et al.* 2005; Sheen 2014). This approach is of interest to better locate noise sources associated to major storms in the Indian Ocean. It is beyond the scope of this study but will deserve some future efforts to improve the accuracy in the noise source locations.

CONCLUSION

We processed 1 yr of continuous data at 15 individual stations from permanent seismic networks within and around the Indian Ocean basin to analyse swell-induced microseismic noise. Time-frequency number of elliptically polarized signals and *BAZ* were used to characterize microseisms, to locate the source areas and to follow their seasonal variability throughout the year 2011.

We showed that both PM and SM are clearly visible in polarization spectra although different processes generate them. We also showed that their source areas are not colocated. SM signals are characterized by seasonal variations with an increase of lower-frequency energy detected in austral winter but stable backazimuth throughout the year pointing towards the South of the Indian Ocean. This result is in good agreement with numerical modelling of SM source areas and can be explained by the closed geometry of the northern part of the ocean basin, which does not allow large microseismic sources to develop in the north of the basin during Northern Hemisphere winters.

From the analysis of 1 yr of data, we showed that time-frequency polarization analysis is an important tool to characterize and locate the swell-induced seismic noise source areas in ocean basins. It may help for instance to identify optimal ocean bottom monitoring sites and to characterize the wave climate changes by analysing much longer periods of recording.

ACKNOWLEDGEMENTS

REFERENCES

Ardhuin, F. *et al.*, 2010. Semiempirical dissipation source functions for ocean waves. Part I: definition, calibration, and validation, *J. Phys. Oceanogr.,* **40**(9), 1917–1941.

Ardhuin, F., Stutzmann, E., Schimmel, M. & Mangeney, A., 2011. Ocean wave sources of seismic noise, *J. geophys. Res.,* **116**(C9), C09004, doi:10.1029/2011JC006952.

Aster, R.C., McNamara, D.E. & Bromirski, P.D., 2008. Multidecadal climate-induced variability in microseisms, *Seism. Res. Lett.,* **79**(2), 194–202.

Banerji, S., 1930. Microseisms associated with disturbed weather in the Indian seas, *Phil. Trans. R. Soc. Lond., A,* **229,** 297–328.

Barruol, G. & Sigloch, K., 2013. Investigating La Réunion hot spot from crust to core, *EOS, Trans. Am. geophys. Un.,* **94**(23), 205–207.

Barruol, G., Reymond, D., Fontaine, F.R., Hyvernaud, O., Maurer, V. & Maamaatuaiahutapu, K., 2006. Characterizing swells in the southern Pacific from seismic and infrasonic noise analyses, *Geophys. J. Int.,* **164**(3), 516–542.

Behr, Y., Townend, J., Bowen, M., Carter, L., Gorman, R., Brooks, L. & Bannister, S., 2013. Source directionality of ambient seismic noise inferred from three-component beamforming, *J. geophys. Res.,* **118,** 240–248.

Bromirski, P.D. & Duennebier, F.K., 2002. The near-coastal microseism spectrum: spatial and temporal wave climate relationships, *J. geophys. Res.,* **107**(B8), doi:10.1029/2001JB000265.

Bromirski, P.D., Duennebier, F.K. & Stephen, R.A., 2005. Mid-ocean microseisms, *Geochem. Geophys. Geosyst.,* **6**(4), Q04009, doi:10.1029/2004GC000768.

Bromirski, P.D., Stephen, R.A. & Gerstoft, P., 2013. Are deep-ocean-generated surface-wave microseisms observed on land?, *J. geophys. Res.,* **118**(7), 3610–3629.

Brooks, L.A., Townend, J., Gerstoft, P., Bannister, S. & Carter, L., 2009. Fundamental and higher-mode Rayleigh wave characteristics of ambient seismic noise in New Zealand, *Geophys. Res. Lett.,* **36,** doi:10.1029/2009GL040434.

Chevrot, S., Sylvander, M., Benahmed, S., Ponsolles, C., Lefevre, J.M. & Paradis, D., 2007. Source locations of secondary microseisms in western Europe: evidence for both coastal and pelagic sources, *J. geophys. Res.,* **112**, B11301, doi:10.1029/2007jb005059.

Davy, C., Barruol, G., Fontaine, F.R., Sigloch, K. & Stutzmann, E., 2014. Tracking major storms from microseismic and hydroacoustic observations on the seafloor, *Geophys. Res. Lett.,* **41,** doi:10.1002/2014GL062319.

Essen, H.H., Krüger, F., Dahm, T. & Grevemeyer, I., 2003. On the generation of secondary microseisms observed in northern and central Europe, *J. geophys. Res.,* **108**(B10), 2506, doi:10.1029/2002JB002338.

Friedrich, A., Kruger, F. & Klinge, K., 1998. Ocean-generated microseismic noise located with the Grafenberg array, *J. Seismol.,* **2**(1), 47–64.

Gerstoft, P. & Tanimoto, T., 2007. A year of microseisms in southern California, *Geophys. Res. Lett.,* **34**, L20304, doi:10.1029/2007gl031091.

Gerstoft, P., Shearer, P., Harmon, N. & Zhang, J., 2008. Gobal P, PP, and PKP wave microseisms observed from distant storms, *Geophys. Res. Lett.,* **35,** doi:10.1029/2008GL036111.

Gualtieri, L., Stutzmann, E., Capdeville, Y., Ardhuin, F., Schimmel, M., Mangeney, A. & Morelli, A., 2013. Modelling secondary microseismic noise by normal mode summation, *Geophys. J. Int.,* **193**(3), 1732–1745.

Gualtieri, L., Stutzmann, E., Farra, V., Capdeville, Y., Schimmel, M., Ardhuin, F. & Morelli, A., 2014. Modelling the ocean site effect on seismic noise body waves, *Geophys. J. Int.,* **197**(2), 1096–1106.

Hasselmann, K., 1963. A statistical analysis of the generation of micro-seisms, *Rev. Geophys.,* **1,** 177–210.

Haubrich, R.A. & McCamy, K., 1969. Microseisms: coastal and pelagic sources, *Rev. Geophys.,* **7,** 539–571.

Haubrich, R.A., Munk, W.H. & Snodgrass, F.E., 1963. Comparative spectra of microseisms and swell, *Bull. seism. Soc. Am.,* **53**(1), 27–37.

Kedar, S., Longuet-Higgins, M.S., Webb, F., Graham, N., Clayton, R. & Jones, C., 2007. The origin of deep ocean microseisms in the north Atlantic ocean, *Proc. R. Soc. A,* **464**(2091), 777–793.

Koper, K.D. & De Foy, B., 2008. Seasonal Anisotropy in Short-Period Seismic Noise Recorded in South Asia, *Bull. seism. Soc. Am.,* **98**(6), 3033–3045.

Koper, K.D., Seats, K. & Benz, H., 2010. On the composition of Earth's short-period seismic noise field, *Bull. seism. Soc. Am.,* **100**(2), 606–617.

Lacoss, R.T., Kelly, E.J. & Toksöz, M.N., 1969. Estimation of seismic noise structure using arrays, *Geophysics,* **34,** 21–38.

Landès, M., Hubans, F., Shapiro, N.M., Paul, A. & Campillo, M., 2010. Origin of deep ocean microseisms by using teleseismic body waves, *J. geophys. Res.,* **115,** B05302, doi:10.1029/2009JB006918.

Lee, A., 1935. On the direction of approach of microseismic waves, *Proc. R. Soc. Lond., A: Math. Phys. Sci.,* **149**(866), 183–199.

Longuet-Higgins, M.S., 1950. A theory of the origin of microseisms, *Phil. Trans. R. Soc. Lond., A,* **243,** 1–35.

Nishida, K., Kawakatsu, H., Fukao, Y. & Obara, K., 2008. Background Love and Rayleigh waves simultaneously generated at the Pacific Ocean floors, *Geophys. Res. Lett.,* **35,** L16307, doi:10.1029/2008gl034753.

Obrebski, M.J., Ardhuin, F., Stutzmann, E. & Schimmel, M., 2012. How moderate sea states can generate loud seismic noise in the deep ocean, *Geophys. Res. Lett.,* **39,** L11601, doi:10.1029/2012gl051896.

Peterson, J., 1993. Observation and modeling of seismic background noise, *U.S. Geol. Surv. Open File Rep,* **93–322,** 1–95.

Ramirez, J., 1940. An experimental investigation of the nature and origin of microseisms at St. Louis; Missouri, Part Two, *Bull. seism. Soc. Am.,* **30,** 139–178.

Reading, A.M., Koper, K.D., Gal, M., Graham, L.S., Tkalčić, H. & Hemer, M.A., 2014. Dominant seismic noise sources in the Southern Ocean and West Pacific, 2000–2012, recorded at the Warramunga Seismic Array, *Geophys. Res. Lett.,* **41,** 3455–3463.

Schimmel, M. & Gallart, J., 2003. The use of instantaneous polarization attributes for seismic signal detection and image enhancement, *Geophys. J. Int.,* **155**(2), 653–668.

Schimmel, M. & Gallart, J., 2004. Degree of polarization filter for frequency-dependent signal enhancement through noise suppression, *Bull. seism. Soc. Am.,* **94**(3), 1016–1035.

Schimmel, M. & Gallart, J., 2005. The inverse S transform in filters with time-frequency localization, *IEEE Trans. Signal Process.,* **53**(11), 4417–4422.

Schimmel, M., Stutzmann, E., Ardhuin, F. & Gallart, J., 2011. Polarized Earth's ambient microseismic noise, *Geochem. Geophys. Geosyst.,* **12,** Q07014, doi:10.1029/2011GC003661.

Sheen, D., 2014. Microseisms from huge Indian Ocean storms in May 2007, *Geosci. J.,* **18**(3), 347–354.

Stockwell, R.G., 1996. Localization of the complex spectrum: the S transform, *IEEE Trans. Signal Process.,* **44**(4), 998–1001.

Stutzmann, E., Ardhuin, F., Schimmel, M., Mangeney, A. & Patau, G., 2012. Modelling long-term seismic noise in various environments, *Geophys. J. Int.,* **191**(2), 707–722.

Stutzmann, E., Schimmel, M., Patau, G. & Maggi, A., 2009. Global climate imprint on seismic noise, *Geochem. Geophys. Geosyst.,* **10,** Q11004, doi:10.1029/2009gc002619.

Tanimoto, T., 2013. Excitation of microseisms: views from the normal-mode approach, *Geophys. J. Int.,* **194,** 1755–1759.

Tanimoto, T. & Alvizuri, C., 2006. Inversion of the HZ ratio of microseisms for *S*-wave velocity in the crust, *Geophys. J. Int.,* **165,** 323–335.

Tanimoto, T., Hadziioannou, C., Igel, H., Wasserman, J., Schreiber, U. & Gebauer, A., 2015. Estimate of Rayleigh-to-Love wave ratio in the secondary microseism by colocated ring laser and seismograph, *Geophys. Res. Lett.,* **42,** doi:10.1002/2015GL063637.

Tanimoto, T., Ishimaru, S. & Alvizuri, C., 2006. Seasonality in particle motion of microseisms, *Geophys. J. Int.,* **166,** 253–266.

Ventosa, S., Simon, C., Schimmel, M., Dañobeitia, J.J. & Manuel, A., 2008. S-transform from a wavelets point of view, *IEEE Trans. Signal Process.,* **56,** 2771–2780.

Webb, S.C. & Crawford, W.C., 2010. Shallow-water broadband OBS seismology, *Bull. seism. Soc. Am.,* **100**(4), 1770–1778.